

Experimental Evidence for Coherent Perfect Absorption in Guided-Mode Resonant Silicon Films

Volume 8, Number 3, June 2016

A. L. Fannin, Student Member, IEEE

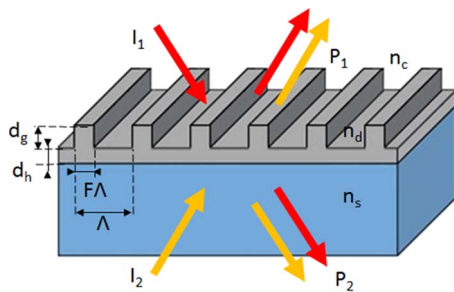
J. W. Yoon

B. R. Wenner

J. W. Allen, Member, IEEE

M. S. Allen, Member, IEEE

R. Magnusson, Life Fellow, IEEE



DOI: 10.1109/JPHOT.2016.2552160

1943-0655 © 2016 IEEE

Experimental Evidence for Coherent Perfect Absorption in Guided-Mode Resonant Silicon Films

A. L. Fannin,^{1,2} *Student Member, IEEE*, J. W. Yoon,¹
B. R. Wenner,² J. W. Allen,³ *Member, IEEE*, M. S. Allen,³ *Member, IEEE*, and
R. Magnusson,¹ *Life Fellow, IEEE*

¹Department of Electrical Engineering, The University of Texas at Arlington,
Arlington, TX 76019 USA

²Air Force Research Laboratory Sensors Directorate, Wright-Patterson Air
Force Base, OH 45433 USA

³Air Force Research Laboratory Munitions Directorate, Eglin Air Force Base, FL 32542 USA

DOI: 10.1109/JPHOT.2016.2552160

1943-0655 © 2016 IEEE. Translations and content mining are permitted for academic research only.
Personal use is also permitted, but republication/redistribution requires IEEE permission.
See http://www.ieee.org/publications_standards/publications/rights/index.html for more information.

Manuscript received December 17, 2015; revised April 4, 2016; accepted April 6, 2016. Date of publication April 7, 2016; date of current version April 21, 2016. This work was supported by a Reliability Information Analysis Center (RIAC) Contract no. HC1047-05-D-4005, TAT 261, with Wyle Laboratories. The work of A. L. Fannin, J. W. Allen, M. S. Allen, and B. R. Wenner was supported by AFOSR Lab Task 14RY15COR (PO: Dr. G. Pomrenke). Corresponding author: R. Magnusson (e-mail: magnusson@uta.edu).

Abstract: We experimentally verify a new class of coherent absorbers based on guided-mode resonance effects in periodic thin films. We design a silicon-based resonant absorber that is fabricated and tested near the 1300-nm wavelength. Implementing phase control, the device can, in principle, be switched between full absorption and full scattering. The first experimental prototype presented herein shows ~78% absorption in the in-phase state. Nearly total scattering is realized in the out-of-phase state. The experimental results agree reasonably well with theory.

Index Terms: Temporal coherence, guided-mode resonance (GMR), subwavelength structures, spatial coherence, absorption, thin-film devices.

1. Introduction

Absorption is among the most fundamental processes that occur when light interacts with matter. It is a basis for practical applications such as detection, laser scribing, and energy generation. Control of absorption in low dimensional material systems such as thin-film geometries is an important and flourishing field of study. In solar energy applications, wideband absorption of incoherent unpolarized light is essential. In that context, Yoon *et al.* demonstrated a 1-D periodic amorphous Si thin-film grating structure that absorbs almost 90% of fully conical unpolarized light across the entire visible spectrum [1]. Cheng *et al.* realized a 2-D periodic silver structure that exhibited nearly perfect absorption of incoherent light by plasmonic resonance in the visible spectral region [2]. Recently, techniques implementing absorption under coherent light interference have gained considerable attention due to several advantages including the use of linear optics and novel functionality not attainable by other means. Thus, the coherent perfect absorber (CPA) concept was proposed by Chong *et al.* to achieve photonic resonance in semiconductor Fabry-Pérot cavities [3]. At about the same time, it was shown by theoretical analysis of

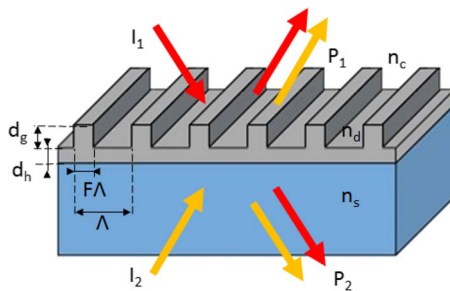


Fig. 1. Architecture of a GMR-based CPA device including key parameters. Ports I_1 and I_2 represent the input beams, while P_1 and P_2 represent output ports. Here, d_g is the grating depth, Δ is the period, F is the fill factor, and d_h is the homogenous sublayer thickness. The cover (air), device (a-Si), and substrate (glass) refractive indices are denoted by n_c , n_d , and n_s , respectively.

a metal grating undergoing plasmonic resonance that total absorption is obtainable in a multiport system by properly configuring input coherent light waves at critical coupling [4]. In ideal CPA devices, two or more input waves totally couple to a single-resonance state and undergo perfect absorption by the intrinsic loss associated with that state. Thus, it was found that complete absorption can be achieved using multiple beams incident on a lossy device such that interference of outgoing beams results in zero outgoing power [3], [4]. As coherent absorbers do not require nonlinear effects to actively modulate light intensity [5], they can be used as low-power active devices such as compact optical switches, modulators, and light-electricity transducers [3]–[7].

CPA has been demonstrated experimentally in flat silicon films [7], periodic metals by surface-plasmonic resonance on a silver grating [8], and in microring resonators [9]. It has also seen exposure in graphene thin films [10] and bilayer structures [11]. Recently, we proposed an alternate approach to CPA in which periodic films are applied. Specifically, we modeled resonant silicon gratings and showed that these are effective in CPA applications [12]. Here, we provide experimental evidence to support these theoretical predictions.

2. Experiments

The experimental results presented apply the guided-mode resonance (GMR) effect as a new basis for coherent perfect absorption. In summary, guided-mode resonance effects arise via quasi-guided, or leaky, waveguide modes induced on patterned films with subwavelength periods [13]–[17]. Simple GMR structures comprising a single 1-D periodic layer have been used to create filters, polarizers, and polarization-independent devices with applications in biosensing, communications, and solar cell enhancement [18]–[20]. Similarly, the GMR concept can easily be adapted into 2-D structures to offer further advantages in each of these applications [21]–[23]. To achieve coherent perfect absorption within a GMR device it is necessary to implement interaction of multiple coherent beams entering the device. The structure of the device determines the wavelengths that are coupled and the angles of coupling. When multiple coherent beams are coupled to the same mode they inherently interfere with one another. This interference can be perfectly constructive, perfectly destructive, or somewhere in-between depending on the phase between two or more beams. In the case of two beams, the phase of one beam can remain fixed while the other one is varied to effectively change the interference interaction. This is the key concept in our design.

Fig. 1 shows the structure of the proposed GMR-based CPA device. The beams labeled I_1 and I_2 are subject to phase control. While it is possible to create any amount of phase difference between 0 and 2π , we address two particular cases where both beams are perfectly in phase or perfectly out of phase. The CPA state occurs as two resonant guided modes separately excited by I_1 and I_2 constructively interfere. Modal energy flowing along the layer is absorbed by the intrinsic loss of the material. This is the ordinary absorption mechanism encountered in a medium with a complex index of refraction $n_d = n + ik$ where the imaginary part k is non-zero.

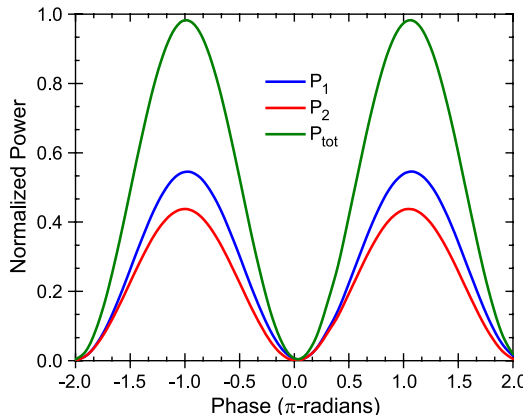


Fig. 2. Theoretical device performance at 1300-nm wavelength, assuming TM polarization. The x-axis represents the phase difference between the two input beams, assuming perfect phase matching at the zero mark. This design assumes an even distribution of power between beams I_1 and I_2 .

Conversely, when the beams are perfectly out of phase, there results destructive interference and effective scattering of the input waves with minimal absorption being possible. These two cases represent nearly perfect absorption and nearly perfect transmission, respectively. Furthermore, it is possible to truncate the level of transmission through the manipulation of the phase. CPA, unlike conventional incoherent absorption, has the added benefit of tunability in the response whereby the resulting output can be modulated using light as control. Absorption can also arise from scattering by rough device surfaces. Atomic-force microscopy (AFM) is employed on our fabricated samples to reveal minimal surface roughness; hence, we believe that absorptive loss by this mechanism is negligible.

We aim to realize a GMR CPA element resonating at $\lambda = 1300$ nm with a 45° incidence of TM-polarized light. Applying numerical design methods, we arrive at a parameter set with a period of 474 nm, a fill factor of 0.26, sublayer thickness of 175 nm, and a grating height of 94 nm assuming $n_d = 3.589 + i0.0127$ for the index of refraction measured by ellipsometry and taking $n_c = 1$. The devices applied in this research are strongly spatially modulated. The spatial modulation strength is defined as $\Delta\epsilon = \text{Re}\{n_d^2 - n_c^2\} = 11.88$. In such strongly modulated devices the transverse leakage out of the illuminated spot is minimal. The device area for all of our fabricated structures is 5 mm by 5 mm. The illuminated spot diameter is approximately 1 mm; thus the spot is well surrounded by the periodic medium. As indicated in Fig. 1, the design consists of amorphous silicon (a-Si) on a SiO_2 substrate. These materials are chosen for their optical properties, wide availability, and simple deposition procedures. Different materials can be used to tailor the characteristics of the device as needed for any specific spectral region.

Fig. 2 shows a theoretical prediction of device performance at wavelength $\lambda = 1300$ nm under TM polarization in which the electric-field vector is parallel to the plane of incidence. It illustrates the phase-sensitive outgoing powers that include the two extreme cases with nearly perfect absorption observed at -2π , 0, and 2π radians and near perfect transmission observed at $-\pi$ and π radians. The absorption state at the phase difference of 0 yields the minimum total outgoing power of $\sim 1\%$ while the transmission state at the phase π shows a maximum of $\sim 98\%$.

The experimental prototype consists of a single layer of a-Si deposited on a glass substrate. A spin-coated photoresist layer is patterned by UV holographic lithography. The a-Si is partially etched, using the developed resist as a mask, to create the grating structure. We characterize the fabricated device with atomic force microscopy with results shown in Fig. 3(a). We find that the fabricated prototype has a period of 474 nm, fill factor of 0.24, and grating height of 103 nm. An additional scanning-electron microscope analysis yields sublayer thickness of 164 nm. Angular measurement confirms that a resonance peak at 45° occurs at $\lambda = 1266$ nm with this prototype device. Fig. 3(b) shows a simplified diagram of the experimental setup used to test the device. A 50/50

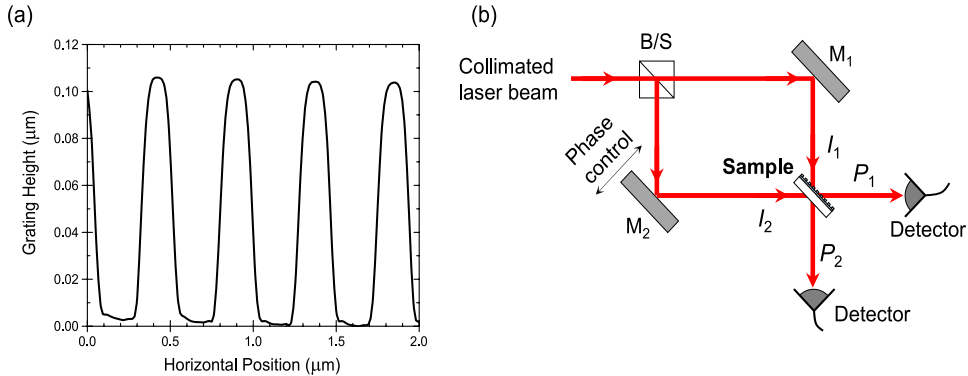


Fig. 3. (a) AFM profile of a fabricated prototype device. (b) Experimental setup to demonstrate CPA. A piezoelectric stage enables phase control of one beam. The axis of displacement for the piezoelectric stage is parallel to the incident beam from the beam splitter.

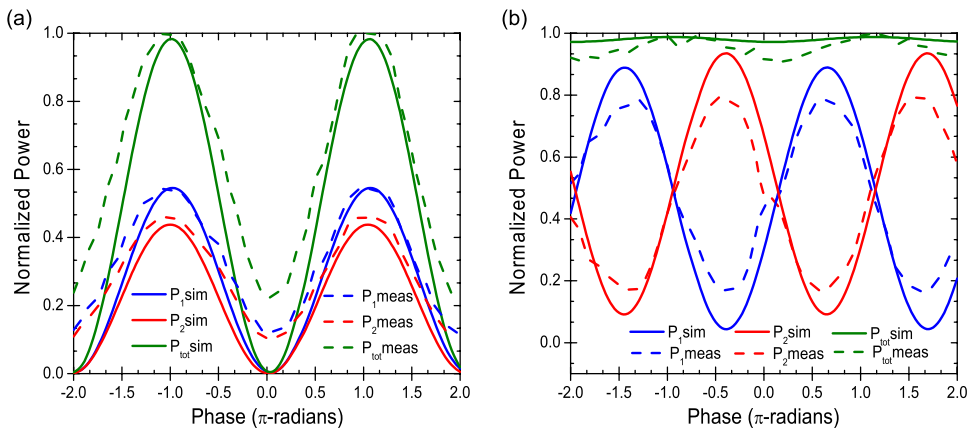


Fig. 4. (a) Measured device performance compared to simulated performance at $\lambda = 1266 \text{ nm}$ under TM polarization. (b) Measured data from the same experiment using a thin film of amorphous silicon with the same thickness and complex refractive index as the device used in part (a).

beam splitter is used for this experiment. Thus, the present design operates at a 1:1 power ratio. The experiment also utilizes an in-line polarizer, a fiber-to-free-space collimator, and a free-space Glan-Taylor polarizer not shown in Fig. 3. The use of both the Glan-Taylor and the in-line polarizer ensures maximum available power for the desired polarization. The sample is mounted on a computer-controlled high-resolution rotation stage for alignment. To account for hysteresis errors in the piezo-electric stage, the data is recorded using ascending voltage values subsequently correlated to displacement. Similar to the rotation stage, the piezo-electric stage is computer controlled.

3. Results

Fig. 4(a) compares theoretical and experimental results for the prototype device. The theoretical model applies the experimental parameters of the fabricated device. It is found that the total power leaving the GMR device in the full-scattering state is $\sim 99\%$ as seen in the figure. This is close to the ideal case of $\sim 98\%$ for our material. In the full-absorption state, the scattered power is at $\sim 22\%$, deviating considerably from the ideal value of $\sim 1\%$. We note that these are initial experimental results and thus the fabricated device does not presently achieve strictly perfect absorption. The reason for the deviation is primarily due to the fact that the laser beams used here have Gaussian profiles and differ considerably from the ideal plane waves with flat phase fronts assumed in the analysis of resonant absorption. We expect that improved collimation of the

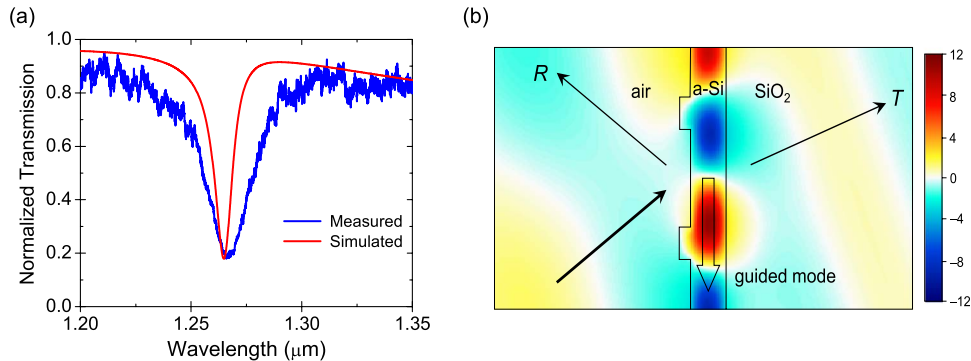


Fig. 5. (a) Comparison of simulated and measured device performance under single-beam excitation at 45° incidence. (b) Simulated internal magnetic fields using the parameters of the fabricated device at $\lambda = 1266 \text{ nm}$.

input beams will lead to results close to the ideal predictions. Additionally, there is some noise in the data as visible in the experimental curves in Fig. 4(a). The noise is mainly due to the high sensitivity of the interferometric optical setup to mechanical vibrations. We note that no detectable amount of power is measured leaving the system through the sides of the device.

As a reference, in the exact same experimental configuration, we substitute the periodic device with a flat layer of a-Si has the same total thickness as the fabricated GMR prototype. The results appear in Fig. 4(b). There is a dramatic difference observed for these two cases. As seen in Fig. 4(b), in stark contrast to the GMR case, there is very minimal absorption as the input power is nearly fully scattered independent of the phase. The fluctuations in Fig. 4(b) account for less than 10% change in the overall power leaving the system.

As the resonantly absorbed power is highly dependent on the phase-sensitive internal field intensity associated with the excited guided mode, it is of interest to examine this point in some detail. A resonance with a high quality factor generally implies strong internal fields and extended photon lifetime which in turn exposes the light to the weakly absorbing material longer, thereby enhancing the absorption. Fig. 5 shows the measured transmittance of the fabricated device in comparison with a computed spectrum using the experimental parameters. There is a finite operating bandwidth with a full-width-at-half-maximum (FWHM) of approximately 10 nm according to the simulation data with the experimental curve being broader. It is within this spectral bandwidth that the proposed absorption occurs. It is possible to design these elements to operate at different central wavelengths. The coherent absorption could thus be shifted to a different spectral location but again the bandwidth would be defined by the device parameters.

Fig. 5(b) shows the computed internal magnetic field profile of the fabricated device under illumination of a single beam at 45° with $\lambda = 1266 \text{ nm}$. The scale bar is set relative to the amplitude of the incident excitation wave assumed to have unit amplitude. There is clearly strong resonant buildup of energy within the device. We note, moreover, that the resonant mode has the shape of the fundamental TM_0 waveguide mode and resides maximally in the sublayer.

4. Conclusion

In summary, we present experimental results illustrating the viability of coherent perfect absorption under guided-mode resonance in nanopatterned thin films with residual, albeit small, loss. Significant levels of resonant in-phase absorption and nearly perfect out-of-phase scattering are shown. These results are contrasted with the absorption and scattering properties of equivalent unpatterned films where only minor absorption is realized for all values of relative phase. Improved experimental conditions implementable by laser beam conditioning are expected to yield experimental data closer to the ideal CPA state.

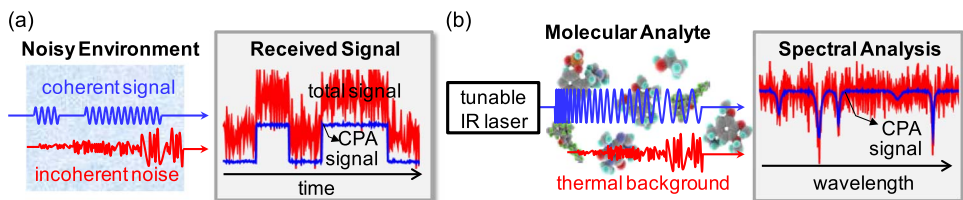


Fig. 6. Potential applications of CPA as a coherent signal filter. (a) Noise suppression in telecommunication signal receivers. (b) Thermal-background-free infrared spectroscopy.

Noise suppression in optical communications and spectroscopic material analysis is a possible application of the GMR CPA effect. As conceptually illustrated in Fig. 6(a), with a CPA photodetector, noise can potentially be filtered by the detector itself without any special noise elimination schemes. Moreover, infrared (IR) spectrometers are important for material composition analysis and hazardous material detection as most molecular species have their own vibrational fingerprints in the IR domain. Thermal background noise can be intense in normal environments at room temperature and an analyte sample itself can act as a strong noise source for IR spectroscopy. This incoherent noise can be filtered by a CPA-integrated photodetection method as schematically depicted in Fig. 6(b). Further study on GMR-CPA integration with existing semiconductor devices may produce novel active optical devices such as optical-to electrical/electrical-to-optical modulators and compact optical amplifiers with a laser diode in CPA configuration.

References

- [1] J. W. Yoon, K. J. Lee, W. Wu, and R. Magnusson, "Wideband omnidirectional polarization-insensitive light absorbers made with 1D silicon gratings," *Adv. Opt. Mater.*, vol. 2, no. 12, pp. 1206–1212, Dec. 2014.
- [2] F. Cheng, J. Gao, T. S. Luk, and X. Yang, "Structural color printing based on plasmonic metasurfaces of perfect light absorption," *Sci. Rep.*, vol. 5, 2015, Art. no. 11045.
- [3] Y. D. Chong, L. Ge, H. Cao, and A. D. Stone, "Coherent perfect absorbers: Time-reversed lasers," *Phys. Rev. Lett.*, vol. 105, no. 5, Jul. 2010, Art. no. 053901.
- [4] J. Yoon, K. H. Seol, S. H. Song, and R. Magnusson, "Critical coupling in dissipative surface-plasmon resonators with multiple ports," *Opt. Exp.*, vol. 18, no. 25, pp. 25702–25711, Dec. 2010.
- [5] J. Zhang, K. F. MacDonald, and N. I. Zheludev, "Controlling light-with-light without nonlinearity," *Light, Sci. Appl.*, vol. 1, p. e18, Jul. 2012.
- [6] X. Fang, K. F. MacDonald, and N. I. Zheludev, "Controlling light with light using coherent metadevices: All-optical transistor, summator, and inverter," *Light, Sci. Appl.*, vol. 4, p. e292, 2015.
- [7] W. Wan *et al.*, "Time-reversed lasing and interferometric control of absorption," *Science*, vol. 331, no. 6019, pp. 889–892, Feb. 2011.
- [8] J. W. Yoon, G. M. Koh, S. H. Song, and R. Magnusson, "Measurement and modeling of a complete optical absorption and scattering by coherent surface plasmon-polariton excitation using a silver thin-film grating," *Phys. Rev. Lett.*, vol. 109, no. 25, Dec. 2012, Art. no. 257402.
- [9] R. R. Grote, J. M. Rothenberg, J. B. Driscoll, and R. M. Osgood, "DPSK demodulation using coherent perfect absorption," in *Proc. IEEE CLEO*, May 2015, pp. 1–2.
- [10] J. Zhang *et al.*, "Coherent perfect absorption and transparency in a nanostructured graphene film," *Opt. Express*, vol. 22, no. 10, pp. 12524–12532, May 2014.
- [11] S. Feng and K. Halterman, "Coherent perfect absorption in epsilon-near-zero metamaterials," *Phys. Rev. B*, vol. 86, no. 16, Oct. 2012, Art. no. 165103.
- [12] J. A. Giese *et al.*, "Guided-mode resonant coherent light absorbers," *Opt. Lett.*, vol. 39, no. 3, pp. 486–488, Feb. 2014.
- [13] P. Vincent and M. Neviere, "Corrugated dielectric waveguides: A numerical study of the second-order stop bands," *Appl. Phys.*, vol. 20, no. 4, pp. 345–351, Dec. 1979.
- [14] L. Mashev and E. Popov, "Zero order anomaly of dielectric coated gratings," *Opt. Comm.*, vol. 55, no. 6, pp. 377–380, Oct. 1985.
- [15] I. A. Avrutsky and V. A. Sychugov, "Reflection of a beam of finite size from a corrugated waveguide," *J. Modern Opt.*, vol. 36, no. 11, pp. 1527–1539, 1989.
- [16] S. S. Wang and R. Magnusson, "Theory and applications of guided-mode resonance filters," *Appl. Opt.*, vol. 32, no. 14, pp. 2606–2613, May 1993.
- [17] S. T. Thurman and G. M. Morris, "Controlling the spectral response in guided-mode resonance filter design," *Appl. Opt.*, vol. 42, no. 16, pp. 3225–3233, Jun. 2003.
- [18] Y. Ding and R. Magnusson, "Resonant leaky-mode spectral-band engineering and device applications," *Opt. Exp.*, vol. 12, no. 23, pp. 5661–5674, Nov. 2004.

- [19] Z. Wang *et al.*, "Guided-mode resonance Brewster filters with multiple channels," *Appl. Phys. Lett.*, vol. 88, no. 25, 2006, Art. no. 251115.
- [20] Y.-C. Lee, C.-F. Huang, J.-Y. Chang, and M.-L. Wu, "Enhanced light trapping based on guided mode resonance effect for thin-film silicon solar cells with two filling-factor gratings," *Opt. Exp.*, vol. 16, no. 11, pp. 7969–7975, May 2008.
- [21] S. Boonruang, A. Greenwell, and M. G. Moharam, "Multiline two-dimensional guided-mode resonant filters," *Appl. Opt.*, vol. 45, no. 22, pp. 5740–5747, Aug. 2006.
- [22] E. Sakat *et al.*, "Free-standing guided-mode resonance band-pass filters: From 1D to 2D structures," *Opt. Exp.*, vol. 20, no. 12, pp. 13082–13090, Jun. 2012.
- [23] W. Zhou *et al.*, "Progress in 2D photonic crystal Fano resonance photonics," *Prog. Quantum Electron.*, vol. 38, no. 1, pp. 1–74, Jan. 2014.